A new sampling indicator function for stable imaging of periodic scattering media

Dinh-Liem Nguyen* Kale Stahl* Trung Truong*

Abstract

This paper is concerned with the inverse problem of determining the shape of penetrable periodic scatterers from scattered field data. We propose a sampling method with a novel indicator function for solving this inverse problem. This indicator function is very simple to implement and robust against noise in the data. The resolution and stability analysis of the indicator function is analyzed. Our numerical study shows that the proposed sampling method is more stable than the factorization method and more efficient than the direct or orthogonality sampling method in reconstructing periodic scatterers.

Keywords. sampling indicator function, inverse scattering, periodic structures, shape reconstruction, photonic crystals

AMS subject classification. 35R30, 78A46, 65C20

1 Introduction

In this paper we aim to numerically solve the inverse scattering problem for periodic media in $\mathbb{R}^2$. The periodic media of interest are unboundedly periodic in the horizontal direction and bounded in the vertical direction. These periodic media are motivated by one-dimensional photonic crystals and the inverse problem of interest is inspired by applications of nondestructive evaluations for photonic crystals. There have been an increasing amount of studies on numerical methods for shape reconstruction of periodic scattering media during the past years, see [1, 2, 4, 6, 9, 11, 15, 20, 22–25, 27, 28]. Two major approaches that were studied in these papers are the factorization method and the near field imaging method. The latter method, which relies on a transformed field expansion, can provide super-resolved resolution. However, this method requires the periodic scattering structure to be a smooth periodic function multiplied by a small surface deformation parameter. The factorization method can essentially work for periodic scattering structures of arbitrary shape but it is not very robust against the noise in the scattering data. This method belongs to the class of sampling or

*Department of Mathematics, Kansas State University, Manhattan, KS 66506; (dlnguyen@ksu.edu, stahlkj@ksu.edu, trungt@ksu.edu)

qualitative methods that were introduced by D. Colton and A. Kirsch [7, 17]. The factorization method aims to construct a necessary and sufficient characterization of the unknown scatterer from multi-static data. We refer to [18] for more details about the factorization method.

In this work we develop a sampling method with a new indicator function to solve the inverse scattering problem for periodic media. This sampling method is inspired by the orthogonality sampling method [26] and the direct sampling method [13]. These two sampling methods share similar ideas and features and were studied independently. For simplicity we will refer to them as the orthogonality sampling method. The computation of the new indicator function is very simple and fast as one only needs to evaluate a finite double sum involving the propagating modes of the scattered field data. Like the orthogonality sampling method, the proposed sampling method also does not involve solving any ill-posed problems and it is very robust against noise in the data. The resolution of the new indicator function is studied using Green's identities and the Rayleigh expansion of the α-quasiperiodic fields of the scattering problem. The stability of the indicator function is also established. The performance of the new indicator function is studied in various contexts in the numerical study. The numerical study also shows that the proposed sampling method is more robust than the factorization method and more efficient than the orthogonality sampling method in reconstructing periodic scattering media. We also want to mention that although the orthogonality sampling method has been studied for inverse scattering from bounded objects [10, 12–14, 16, 19, 26], its application to the inverse scattering problem for periodic media is still not known.

The paper is organized as follows. The basics of the scattering from periodic media and the inverse problem of interest are described in Section 2. The new indicator function and its resolution and stability analysis are discussed in Section 3. Section 4 is dedicated to a numerical study of the new indicator function and its comparison to the factorization method and the orthogonality sampling method.

2 Problem setup

We consider a two-dimensional medium which is unboundedly 2π-periodic in x_1-direction and bounded in x_2-direction. Let n be a bounded function which is 2π-periodic with respect to x_1. Suppose that the interior of the periodic medium is characterized by n and that the exterior of the periodic medium is homogeneous which means $n = 1$ in these areas. Note that the period can be any arbitrary value, but it is chosen to be 2π for the convenience of the presentation. For $\alpha \in \mathbb{R}$, we define that a function f is α-quasiperiodic in x_1 if

$$f(x_1 + 2\pi j, x_2) = \mathrm{e}^{i2\pi j\alpha} f(x_1, x_2), \quad j \in \mathbb{Z}, \quad (x_1, x_2)^\top \in \mathbb{R}^2.$$

From now on we will call functions with this property α-quasiperiodic functions for short. A typical example of α-quasiperiodic functions is a plane wave (e.g. $\exp(ik(d_1x_1 + d_2x_2))$ with $d_1^2 + d_2^2 = 1$, $k > 0$). Suppose that the periodic medium is illuminated by an α-quasiperiodic incident field u_{in} with wave number $k > 0$. Note that since the medium is

unboundedly periodic in x_1, we are only interested incident fields propagating downward or upward toward the medium. The scattering of such an incident field by the periodic medium produces the scattered field u_{sc} described by

$$\Delta u_{sc} + k^2 u_{sc} = -k^2 q u \quad \text{in } \mathbb{R}^2, \tag{1}$$

where $u := u_{sc} + u_{in}$ is the total field and q is the contrast given by

$$q = n - 1.$$

We follow the usual approach in that for the well-posedness of the direct scattering problem we look for an α-quasiperiodic scattered field u_{sc} (see [5]). Thus, the direct problem of finding u_{sc} can be reduced to one period

$$\Omega := (-\pi, \pi) \times \mathbb{R}.$$

Let $D = \text{supp}(q) \cap \Omega$. For $h > 0$ such that

$$h > \sup\big\{|x_2| : (x_1, x_2)^\top \in D\big\}, \tag{2}$$

the direct scattering problem is completed by the Rayleigh expansion condition for the scattered field

$$u_{sc}(x) = \begin{cases} \sum_{j\in\mathbb{Z}} u_j^+ \mathrm{e}^{i\alpha_j x_1 + i\beta_j (x_2 - h)}, & x_2 \geq h, \\ \sum_{j\in\mathbb{Z}} u_j^- \mathrm{e}^{i\alpha_j x_1 - i\beta_j (x_2 + h)}, & x_2 \leq -h, \end{cases} \tag{3}$$

where

$$\alpha_j := \alpha + j, \quad \beta_j := \begin{cases} \sqrt{k^2 - \alpha_j^2}, & k^2 \geq \alpha_j^2 \\ i\sqrt{\alpha_j^2 - k^2}, & k^2 < \alpha_j^2 \end{cases}, \quad j \in \mathbb{Z},$$

and $(u_j^\pm)_{j\in\mathbb{Z}}$ are the (complex-valued) Rayleigh sequences of the scattered field u_{sc}. The condition (3) means that the scattered field u_{sc} is an outgoing wave. Note that only a finite number of terms in (3) are propagating plane waves which are called propagating modes, the rest are evanescent modes which correspond to exponentially decaying terms. From now, we call a function satisfying (3) a radiating function. In addition, we also assume that β_j is nonzero for all j which means the Wood anomalies are excluded in our analysis.

With the further assumption that $n(x) > c$ almost everywhere for some positive constant c, the scattering problem (1)–(3) is well-posed for all but a countable set of wave numbers k, see [5]. In this paper we always assume the wave number k such that the direct problem is well-posed. For $r > 0$ define

$$\Omega_r := (-\pi, \pi) \times (-r, r), \quad \Gamma_{\pm r} := (-\pi, \pi) \times \{\pm r\}.$$

Recall the constant h in (2). For the inverse problem of interest we measure the scattered field u_{sc} on $\Gamma_{\pm r}$ for some $r \geq h$. From the Rayleigh expansion of u_{sc}, knowing u_{sc} on $\Gamma_{\pm r}$ is equivalent to knowing the Rayleigh coefficients $(u_j^\pm)_{j\in\mathbb{Z}}$. Since the evanescent modes are

associated with the exponentially decaying terms in the Rayleigh expansion (3), it is typically difficult to obtain these modes in practice unless one can measure extremely near (e.g. within one wavelength) the periodic scatterers. Thus, we consider only the propagating modes for the scattering data of our inverse problem as follows.

Inverse problem. Given the Rayleigh coefficients $(u_j^{\pm})$ for $j \in \mathbb{Z}$ such that $\beta_j > 0$, determine D.

3 A new indicator function and its properties

It is well-known that the α-quasiperiodic Green function of the direct problem is given by

$$G_{k,\alpha}(x,y) = \frac{i}{4\pi} \sum_{j\in\mathbb{Z}} \frac{1}{\beta_j} \mathrm{e}^{i\alpha_j(x_1-y_1)+i\beta_j|x_2-y_2|}, \quad x, y \in \Omega,\, x_2 \neq y_2. \tag{4}$$

We refer to [3] for a derivation and more details on the α-quasiperiodic Green function of the direct problem. We also refer to [8] for the fact that the direct problem is equivalent to the Lippmann-Schwinger equation

$$u_{sc}(x) = k^2 \int_D G_{k,\alpha}(x,y) q(y) u(y)\, dy. \tag{5}$$

Let N be the number of incident fields we use for the inverse problem. The incident fields can be either point sources $G_{\alpha,k}(\cdot, y_l)$ or plane waves $\exp(i\alpha_l x_1 + i\beta_l x_2)$ for $l = 1, 2, \ldots, N$. Let $u_j^{\pm}(l)$ be the Rayleigh coefficients of the scattered field $u_{sc}(\cdot, l)$ generated by incident field $u_{in}(\cdot, l)$ for $l = 1, 2, \ldots, N$. For $p \in \mathbb{N}, z \in \Omega$, define the following indicator function

$$I(z) := \sum_{l=1}^{N} \left| \sum_{j:\beta_j>0} \beta_j \left(u_j^+(l)\overline{g_j^+(z)} + u_j^-(l)\overline{g_j^-(z)} \right) \right|^p, \tag{6}$$

where

$$g_j^{\pm}(z) = \frac{i}{4\pi\beta_j} \mathrm{e}^{-i\alpha_j z_1 \mp i\beta_j(z_2 \mp h)}.$$

This indicator function $I(z)$ aims to determine D in Ω and z plays the role of sampling points. We note that $g_j^{\pm}(z)$ are also the Rayleigh coefficients of the α-quasiperiodic Green function. In the proof of following theorem we will drop the dependence of $u_j^{\pm}$ on l for the convenience of the presentation but we keep l in the total field $u(y, l)$ that is generated by incident field $u_{in}(y, l)$. We analyze the behavior of $I(z)$ in the following theorem.

Theorem 1. *The indicator function satisfies*

$$I(z) = \left(\frac{k^2}{8\pi}\right)^p \sum_{l=1}^{N} \left| \int_D \left[J_0(k|z-y|) + w_\alpha(z,y) \right] q(y) u(y,l) dy \right|^p$$

where J_0 is the Bessel function of the first kind, and

$$w_\alpha(z,y) := \sum_{j\in\mathbb{Z}\setminus\{0\}} e^{-i2\pi j\alpha} J_0\left(k\sqrt{(z_1-y_1+2j\pi)^2 + (z_2-y_2)^2} \right). \tag{7}$$

Remark 2. *The series in (7) converges due to the decay of* $J_0(k\sqrt{(z_1-y_1+2j\pi)^2+(z_2-y_2)^2})$. *We numerically observe that the kernel function* $J_0(k|z-y|)+w_\alpha(z,y)$ *peaks at* $z=y$ *and is relatively small as* y *and* z *are away from each other, see Figure 1 for an example. Thus we expect from the theorem that* $I(z)$ *has small values as* z *is outside* D *and has much larger values as* z *is inside* D.

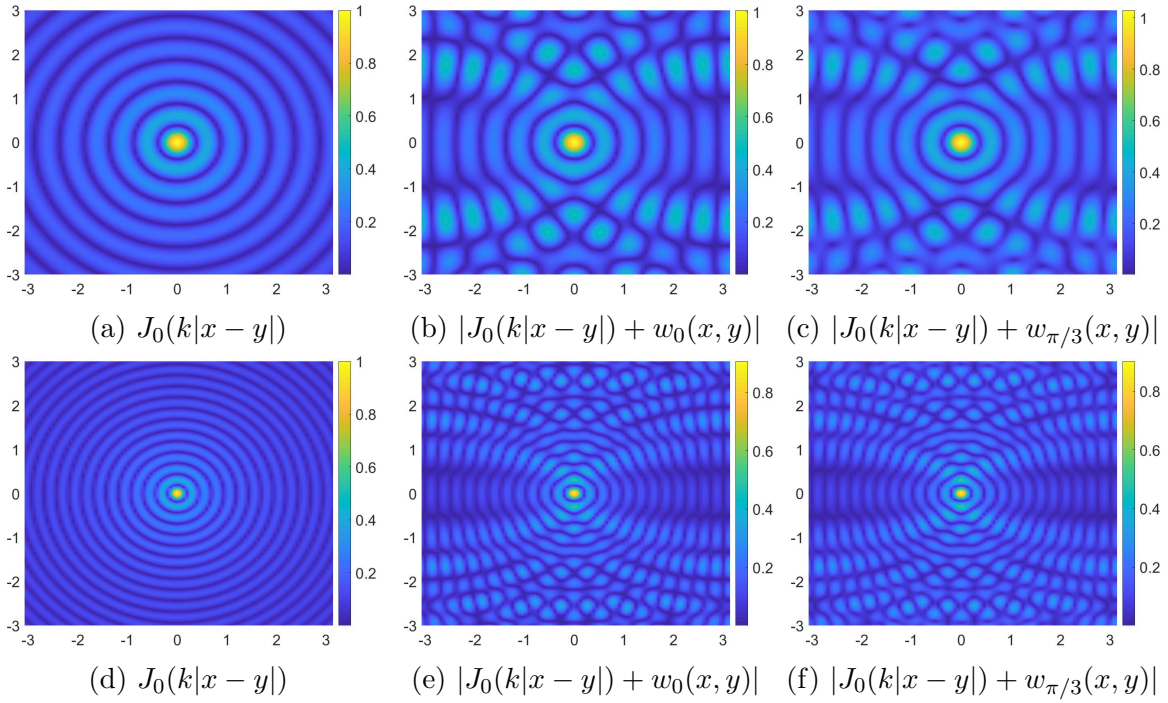

(a) $J_0(k|x-y|)$ (b) $|J_0(k|x-y|)+w_0(x,y)|$ (c) $|J_0(k|x-y|)+w_{\pi/3}(x,y)|$

(d) $J_0(k|x-y|)$ (e) $|J_0(k|x-y|)+w_0(x,y)|$ (f) $|J_0(k|x-y|)+w_{\pi/3}(x,y)|$

Figure 1: Functions $J_0(k|x-y|)$ and $|J_0(k|x-y|)+w_\alpha(x,y)|$ for $x\in(-\pi,\pi)\times(-3,3)$, $y=0$, $k=2\pi$ (first row) and $k=4\pi$ (second row).

Proof. For $x_s\in\Omega_h$, $G_{k,\alpha}(x,x_s)$ solves

$$\Delta G_{k,\alpha}(x,x_s)+k^2G_{k,\alpha}(x,x_s)=-\delta(x-x_s),\quad x\in\Omega_h.$$

For $x_t\in\Omega_h$, multiplying both sides by $\overline{G_{k,\alpha}(x,x_t)}$ and integrating over Ω_h gives

$$\int_{\Omega_h}(\Delta G_{k,\alpha}(x,x_s)+k^2G_{k,\alpha}(x,x_s))\overline{G_{k,\alpha}(x,x_t)}\,dx=-\overline{G_{k,\alpha}(x_s,x_t)}. \tag{8}$$

Similarly, $\overline{G_{k,\alpha}(x,x_t)}$ solves

$$\Delta\overline{G_{k,\alpha}(x,x_t)}+k^2\overline{G_{k,\alpha}(x,x_t)}=-\delta(x-x_t),\quad x\in\Omega_h,$$

thus by multiplying both sides by $G_{k,\alpha}(x,x_s)$ and integrating over Ω_h we obtain

$$\int_{\Omega_h}(\Delta\overline{G_{k,\alpha}(x,x_t)}+k^2\overline{G_{k,\alpha}(x,x_t)})G_{k,\alpha}(x,x_s)\,dx=-G_{k,\alpha}(x_t,x_s). \tag{9}$$

Subtracting (9) from (8) yields

$$G_{k,\alpha}(x_t,x_s)-\overline{G_{k,\alpha}(x_s,x_t)}=\int_{\Omega_h}\Delta G_{k,\alpha}(x,x_s)\overline{G_{k,\alpha}(x,x_t)}-\Delta\overline{G_{k,\alpha}(x,x_t)}G_{k,\alpha}(x,x_s)\,dx$$
$$=\int_{\partial\Omega_h}\overline{G_{k,\alpha}(x,x_t)}\frac{\partial G_{k,\alpha}(x,x_s)}{\partial\nu}-G_{k,\alpha}(x,x_s)\frac{\partial\overline{G_{k,\alpha}(x,x_t)}}{\partial\nu}\,ds(x),$$

where ν is an unit normal outward vector to $\partial\Omega_h$. Thanks to the α-quasiperiodicity of $G_{k,\alpha}$ we have that

$$\int_{\{\pm\pi\}\times(-h,h)}\overline{G_{k,\alpha}(x,x_t)}\frac{\partial G_{k,\alpha}(x,x_s)}{\partial\nu}-G_{k,\alpha}(x,x_s)\frac{\partial\overline{G_{k,\alpha}(x,x_t)}}{\partial\nu}\,ds(x)=0.$$

Therefore

$$G_{k,\alpha}(x_t,x_s)-\overline{G_{k,\alpha}(x_s,x_t)}=\int_{\Gamma_h\cup\Gamma_{-h}}\overline{G_{k,\alpha}(x,x_t)}\frac{\partial G_{k,\alpha}(x,x_s)}{\partial\nu}-G_{k,\alpha}(x,x_s)\frac{\partial\overline{G_{k,\alpha}(x,x_t)}}{\partial\nu}\,ds(x).\tag{10}$$

Define

$$F(x,y):=\frac{G_{k,\alpha}(x,y)-\overline{G_{k,\alpha}(y,x)}}{2i},\qquad x,y\in\Omega_h,$$

then the left-hand side of (10) equals $2iF(x_t,x_s)$. Now we calculate the right-hand side. Since $G_{k,\alpha}$ satisfies the radiation condition, for a fixed $y\in\Omega_h$,

$$G_{k,\alpha}(x,y)=\sum_{j\in\mathbb{Z}}g_j^{\pm}(y)e^{i\alpha_j x_1},\ x\in\Gamma_{\pm h}\tag{11}$$

and

$$\frac{\partial G_{k,\alpha}(x,y)}{\partial\nu}=\sum_{j\in\mathbb{Z}}i\beta_j g_j^{\pm}(y)e^{i\alpha_j x_1},\ x\in\Gamma_{\pm h}.$$

Therefore

$$\int_{\Gamma_{\pm h}}\overline{G_{k,\alpha}(x,x_t)}\frac{\partial G_{k,\alpha}(x,x_s)}{\partial\nu}\,ds(x)=\int_{-\pi}^{\pi}\sum_{j_1,j_2\in\mathbb{Z}}i\beta_{j_2}\overline{g_{j_1}^{\pm}(x_t)}g_{j_2}^{\pm}(x_s)e^{i(\alpha_{j_2}-\alpha_{j_1})x_1}\,dx_1$$
$$=\sum_{j_1,j_2\in\mathbb{Z}}i\beta_{j_2}\overline{g_{j_1}^{\pm}(x_t)}g_{j_2}^{\pm}(x_s)\int_{-\pi}^{\pi}e^{i(j_2-j_1)x_1}\,dx_1,$$

and since

$$\int_{-\pi}^{\pi}e^{i(j_2-j_1)x_1}\,dx_1=\begin{cases}2\pi, & j_1=j_2\\ 0, & j_1\neq j_2\end{cases}$$

we have

$$\int_{\Gamma_h\cup\Gamma_{-h}}\overline{G_{k,\alpha}(x,x_t)}\frac{\partial G_{k,\alpha}(x,x_s)}{\partial\nu}\,ds(x)=2\pi i\sum_{j\in\mathbb{Z}}\beta_j\left(\overline{g_j^{+}(x_t)}g_j^{+}(x_s)+\overline{g_j^{-}(x_t)}g_j^{-}(x_s)\right).\tag{12}$$

Similarly

$$\int_{\Gamma_h \cup \Gamma_{-h}} G_{k,\alpha}(x, x_s) \frac{\partial \overline{G_{k,\alpha}(x, x_t)}}{\partial \nu} \, ds(x) = -2\pi i \sum_{j \in \mathbb{Z}} \overline{\beta_j} \left(\overline{g_j^+(x_t)} g_j^+(x_s) + \overline{g_j^-(x_t)} g_j^-(x_s) \right). \quad (13)$$

Combining (12) and (13) yields

$$G_{k,\alpha}(x_t, x_s) - \overline{G_{k,\alpha}(x_s, x_t)} = 2\pi i \sum_{j \in \mathbb{Z}} (\beta_j + \overline{\beta_j}) \left(\overline{g_j^+(x_t)} g_j^+(x_s) + \overline{g_j^-(x_t)} g_j^-(x_s) \right),$$

that is

$$F(x_t, x_s) = 2\pi \sum_{j \in \mathbb{Z}} \operatorname{Re} \beta_j \left(\overline{g_j^+(x_t)} g_j^+(x_s) + \overline{g_j^-(x_t)} g_j^-(x_s) \right). \quad (14)$$

From the Rayleigh expansion (3) we have that

$$u_j^{\pm} = \frac{1}{2\pi} \int_{\Gamma_{\pm h}} u_{sc}(x) e^{-i\alpha_j x_1} ds(x).$$

Thus, for $j \in \mathbb{Z}$, substituting (5) into the integral above gives

$$\begin{aligned} u_j^{\pm} &= \frac{1}{2\pi} \int_{\Gamma_{\pm h}} \left(k^2 \int_D G_{k,\alpha}(x, y) q(y) u(y) \, dy \right) e^{-i\alpha_j x_1} \, ds(x) \\ &= k^2 \int_D \left(\frac{1}{2\pi} \int_{\Gamma_{\pm}} G_{k,\alpha}(x, y) e^{-i\alpha_j x_1} \, ds(x) \right) q(y) u(y) \, dy = k^2 \int_D g_j^{\pm}(y) q(y) u(y) \, dy. \end{aligned}$$

For $z \in \Omega$, using the Rayleigh coefficients of $u_j^{\pm}$ above and (14) we obtain

$$\begin{aligned} & 2\pi \sum_{j \in \mathbb{Z}} \operatorname{Re} \beta_j \left(u_j^+ \overline{g_j^+(z)} + u_j^- \overline{g_j^-(z)} \right) \\ &= k^2 \int_D 2\pi \sum_{j \in \mathbb{Z}} \operatorname{Re} \beta_j \left(g_j^+(y) \overline{g_j^+(z)} + g_j^-(y) \overline{g_j^-(z)} \right) q(y) u(y) \, dy \\ &= k^2 \int_D F(z, y) q(y) u(y) \, dy. \end{aligned} \quad (15)$$

Now, using the following representation of the α-quasiperiodic Green function

$$G_{k,\alpha}(z, y) = \frac{i}{4} \sum_{j \in \mathbb{Z}} e^{-i2\pi j\alpha} H_0^{(1)} \left(k \sqrt{(z_1 - y_1 + 2j\pi)^2 + (z_2 - y_2)^2} \right)$$

where the series converges for $(y_1 - z_1, y_2 - z_2) \neq (2j\pi, 0)$, $j \in \mathbb{Z}$, we have

$$\begin{aligned} F(z, y) &= \frac{1}{8} \sum_{j \in \mathbb{Z}} e^{-i2\pi j\alpha} H_0^{(1)} \left(k \sqrt{(z_1 - y_1 + 2j\pi)^2 + (z_2 - y_2)^2} \right) \\ &\quad + \frac{1}{8} \sum_{j \in \mathbb{Z}} e^{i2\pi j\alpha} \overline{H_0^{(1)} \left(k \sqrt{(y_1 - z_1 + 2j\pi)^2 + (y_2 - z_2)^2} \right)} \\ &= \frac{1}{4} \sum_{j \in \mathbb{Z}} e^{-i2\pi j\alpha} J_0 \left(k \sqrt{(z_1 - y_1 + 2j\pi)^2 + (z_2 - y_2)^2} \right). \end{aligned}$$

Also from the definition of $I(z)$ in (6) and the equation (15) we obtain

$$I(z) = \sum_{l=1}^{N} \left| \frac{k^2}{2\pi} \int_D F(z,y) q(y) u(y)\, dy \right|^p .$$

Substituting the representation of $F(z,y)$ above we complete the proof of the theorem. □

In the next theorem we will establish a stability estimate for the indicator function. Assume $u_{sc}(\cdot,l) \in L^2(\Gamma_r \cup \Gamma_{-r})$ for all $l = 1,\dots,N$.

Theorem 3. *For $\delta > 0$, denote by $u_{sc,\delta}$ and $\left(u^{\pm}_{\delta,j}\right)_{j\in\mathbb{Z}}$ the noisy scattered wave and its Rayleigh sequences respectively, for which we have*

$$\sum_{l=1}^{N} \|u_{sc,\delta}(\cdot,l) - u_{sc}(\cdot,l)\|_{L^2(\Gamma_r\cup\Gamma_{-r})} \le \delta.$$

Define

$$I_\delta(z) := \sum_{l=1}^{N} \left| \sum_{j:\beta_j>0} \beta_j \left(u^+_{\delta,j}(l)\overline{g^+_j(z)} + u^-_{\delta,j}(l)\overline{g^-_j(z)} \right) \right|^p .$$

Then the following stability property holds

$$|I_\delta(z) - I(z)| = O(\delta), \quad \text{as } \delta \to 0$$

for every $z \in \Omega$.

Proof. For $l = 1,\dots,N$ and $j \in \mathbb{Z}$ such that $\beta_j > 0$, we have

$$|u^{\pm}_{\delta,j}(l) - u^{\pm}_j(l)| \le \frac{1}{2\pi} \int_{\Gamma_{\pm r}} |u^{\delta}_{sc}(x,l) - u_{sc}(x,l)|\, ds(x),$$

thus, by Cauchy-Schwarz inequality,

$$\sum_{l=1}^{N} |u^{\pm}_{\delta,j}(l) - u^{\pm}_j(l)| \le \sum_{l=1}^{N} \|u^{\delta}_{sc}(\cdot,l) - u_{sc}(\cdot,l)\|_{L^2(\Gamma_r\cup\Gamma_{-r})} \le \delta.$$

Therefore

$$\begin{aligned}
&\left| \sum_{l=1}^{N} \left| \sum_{j:\beta_j>0} \beta_j \left(u^+_{\delta,j}(l)\overline{g^+_j(z)} + u^-_{\delta,j}(l)\overline{g^-_j(z)} \right) \right| - \sum_{l=1}^{N} \left| \sum_{j:\beta_j>0} \beta_j \left(u^+_j(l)\overline{g^+_j(z)} + u^-_j(l)\overline{g^-_j(z)} \right) \right| \right| \\
&\le \sum_{l=1}^{N} \left| \left| \sum_{j:\beta_j>0} \beta_j \left(u^+_{\delta,j}(l)\overline{g^+_j(z)} + u^-_{\delta,j}(l)\overline{g^-_j(z)} \right) \right| - \left| \sum_{j:\beta_j>0} \beta_j \left(u^+_j(l)\overline{g^+_j(z)} + u^-_j(l)\overline{g^-_j(z)} \right) \right| \right| \\
&\le \sum_{l=1}^{N} \sum_{j:\beta_j>0} \beta_j \left(\left|u^+_{\delta,j}(l) - u^+_j(l)\right| \left|g^+_j(z)\right| + \left|u^-_{\delta,j}(l) - u^-_j(l)\right| \left|g^-_j(z)\right| \right) \\
&\le C\delta,
\end{aligned}$$

where

$$C = \left(\max_{j:\beta_j>0} \left\| g_j^+ \right\|_{L^\infty(\Omega)} + \max_{j:\beta_j>0} \left\| g_j^- \right\|_{L^\infty(\Omega)} \right) \sum_{j:\beta_j>0} \beta_j.$$

For brevity, set

$$\begin{aligned}
a_l &:= \left| \sum_{j:\beta_j>0} \beta_j \left(u_{\delta,j}^+(l) \overline{g_j^+(z)} + u_{\delta,j}^-(l) \overline{g_j^-(z)} \right) \right|, \\
b_l &:= \left| \sum_{j:\beta_j>0} \beta_j \left(u_j^+(l) \overline{g_j^+(z)} + u_j^-(l) \overline{g_j^-(z)} \right) \right|, \\
\gamma &:= \max_{\substack{j:\beta_j>0 \\ l=1,\dots,N}} \left\{ \left| u_j^+(l) \right|, \left| u_j^-(l) \right| \right\},
\end{aligned}$$

then we have

$$\sum_{l=1}^{N} |a_l - b_l| \le C\delta, \quad b_l \le C\gamma,$$

for all $l = 1, \dots, N$. Hence, for all $z \in \Omega$,

$$\begin{aligned}
|I_\delta(z) - I(z)| &\le \sum_{l=1}^{N} |a_l^p - b_l^p| = \sum_{l=1}^{N} \left(|a_l - b_l| \left| \sum_{m=0}^{p-1} a_l^m b_l^{p-1-m} \right| \right) \\
&\le \left(\sum_{l=1}^{N} |a_l - b_l| \right) \left(\sum_{l=1}^{N} \left| \sum_{m=0}^{p-1} a_l^m b_l^{p-1-m} \right| \right) \\
&\le C\delta \sum_{l=1}^{N} \sum_{m=0}^{p-1} (|a_l - b_l| + b_l)^m b_l^{p-1-m} \\
&\le C\delta \sum_{l=1}^{N} \sum_{m=0}^{p-1} 2^m (|a_l - b_l|^m + b_l^m) b_l^{p-1-m} \\
&\le C\delta \sum_{m=0}^{p-1} \sum_{l=1}^{N} 2^m (|a_l - b_l|^m + \gamma^m) \gamma^{p-1-m} \\
&\le C\delta \sum_{m=0}^{p-1} 2^m \left(C^m \delta^m \gamma^{p-1-m} + N\gamma^{p-1} \right) \\
&= O(\delta), \quad \text{as } \delta \to 0.
\end{aligned}$$

This completes the proof. □

4 Numerical study

In this section, we test the performance of the proposed sampling method with respect to the number of incident sources, the levels of noise in the data, the wave numbers, the values

of parameter α (in (3)) and exponent p, and the shape of the periodic scatterers. For the latter category we compare the performance of the proposed sampling method with those of the factorization method and the orthogonality sampling method.

In all of the numerical examples below we choose the following parameters:

$$\begin{aligned} \text{sampling domain} &= (-\pi,\pi)\times(-1,1),\ h=1,\\ \text{measurement boundary}\quad \Gamma_{\pm 2} &= (-\pi,\pi)\times\{\pm 2\},\\ \text{location of incident sources}\quad \Gamma_{\pm 3} &= (-\pi,\pi)\times\{\pm 3\}. \end{aligned}$$

In our numerical study we observed that any reasonable choices of these parameters do not affect much the performance of the method. The sampling domain is uniformly discretized in each dimension with 128×96 sampling points. The boundary measurements $\Gamma_{\pm 2}$ are discretized uniformly with 64 points on each boundary. By using N incident sources we mean to consider

$$u_{in}(x,l)=G_{k,\alpha}(x,y_l),\quad x\in\Omega,\quad y_l\in\Gamma_{\pm 3},\ l=1,\dots,N,$$

where $N/2$ sources are uniformly located on Γ_{+3} and $N/2$ sources are uniformly located on Γ_{-3}. For a source $G_{k,\alpha}(x,y)$ located on Γ_{+3}, we can see for $y_2<3$ that $G_{k,\alpha}(x,y)$ is a series of downward propagating plane waves and exponentially decaying evanescent waves. Similarly, for a source located on Γ_{-3}, $G_{k,\alpha}(x,y)$ is a series of upward propagating plane waves and and exponentially decaying evanescent waves for $y>-3$. Figure 2 presents the real and imaginary parts of a source on Γ_3.

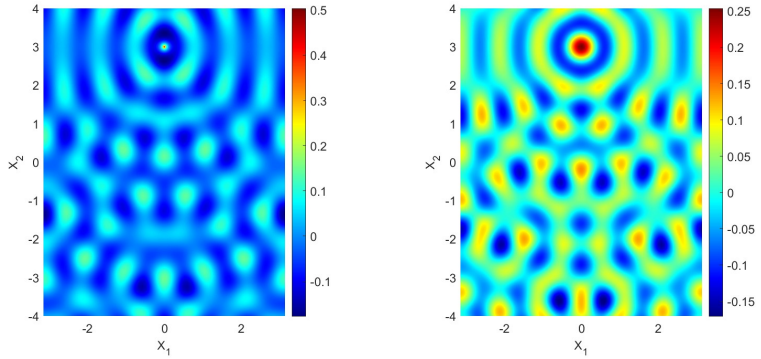

Figure 2: The real (left) and imaginary (right) parts of the source $G_{k,\alpha}(x,y)$ with $y=(0,3)^T$, $x\in(-\pi,\pi)\times(-4,4)$, $k=2\pi,\alpha=0$.

We generate the synthetic scattering data by solving the direct problem with the spectral Galerkin method studied in [21]. The entries of the artificial noise matrix are of the form $a+ib$ where real scalars $a,b\in(-1,1)$ are generated randomly with a uniform distribution. With the artificial noise added to the synthetic scattering data we implement the indicator function

$$I_\delta(z)=\sum_{l=1}^{N}\left|\sum_{j:\beta_j>0}\beta_j\left(u^+_{\delta,j}(l)\overline{g_j^+(z)}+u^-_{\delta,j}(l)\overline{g_j^-(z)}\right)\right|^p.$$

To compare with the orthogonality sampling method we implement following indicator function

$$I_{OSM}(z) = \sum_{l=1}^{N} \left| \int_{\Gamma_{+2} \cup \Gamma_{-2}} u_{sc,\delta}(x) \, \overline{G_{k,\alpha}(x,z)} ds(x) \right|^p .$$

This indicator function of the orthogonality sampling method can be rewritten in the modal form by using the Rayleigh expansion of the scattered field. In this modal form the evanescent modes or the exponentially decaying terms can be neglected and there remains only a finite number of the propagating modes. If we drop β_j in $I_\delta(z)$, we will approximately obtain the modal form of $I_{OSM}(z)$. We refer to [22] for the indicator function of the factorization method implemented for the test in this section.

4.1 Reconstruction with one incident source (Figure 3)

In this section we test the performance of the sampling method for data generated by only one incident source. Here the parameters are chosen as $\alpha = 0$, wave number $k = 2\pi$, and exponent $p = 4$. We add 20% artificial noise to the scattered field data ($\delta = 20\%$). From Figure 3 we can see that the method is able to reconstruct small scatterers quite well. This capability is an advantage over classical sampling methods (e.g. linear sampling method, factorization method) in terms of computational efficiency since classical methods are only able to reconstruct targets with data generated by multiple incident fields. However, the proposed sampling method fails to reconstruct scatterers with extended shape, which is reasonable since only one incident source and one wave number are used for the data. We refer to Figure 4 for improved results when multiple incident sources are used for the reconstruction.

4.2 Reconstruction with multiple incident sources (Figure 4)

In this section we test the performance of the method for reconstructing extended scatterers with different number of incident sources. The parameters are the same as in Figure 3, meaning $\alpha = 0$, wave number $k = 2\pi$, exponent $p = 4$, and 20% artificial noise is added to the scattered field data. If in Figure 3 the method fails to reconstruct extended ellipses with one incident source, the reconstructions are improved with more sources, see Figure 4. The reconstructions already look reasonable with 32 incident sources and continue to improve when more sources are used. The results remain almost the same even if more than 128 incident sources are used to generate the scattering data.

4.3 Reconstruction with different levels of noise in the data (Figure 5)

In this section we test the performance of the method for reconstructing extended scatterers with different levels of artificial noise in the data (10%, 20% and 40%). Here the parameters are chosen as $\alpha = 0$, wave number $k = 2\pi$, exponent $p = 4$, and 128 incident sources are used to generate the scattering data. It can be seen from Figure 5 that all reconstructions

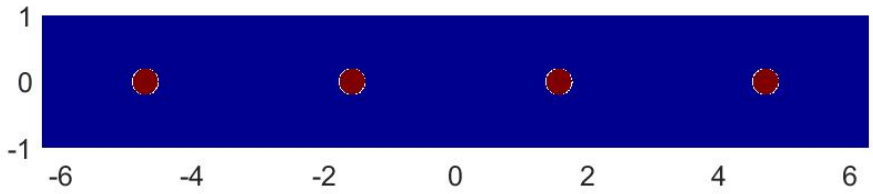

(a) True geometry in $(-2\pi, 2\pi)$.

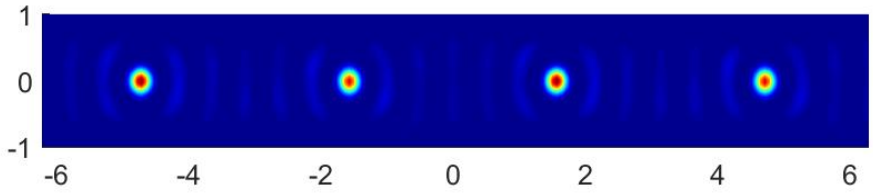

(b) Reconstruction of small elliptical scatterers in Figure 3-(a).

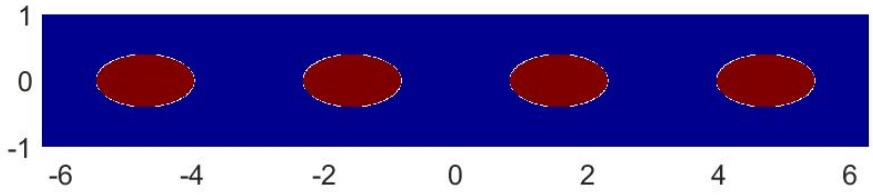

(c) True geometry in $(-2\pi, 2\pi)$.

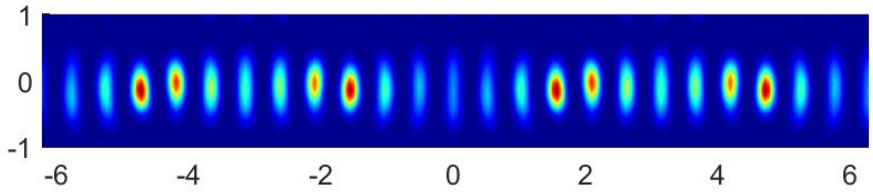

(d) Reconstruction of extended elliptical scatterers in Figure 3-(c).

Figure 3: Reconstruction of small and extended elliptical scatterers with one incident source.

are not affected by the amounts of noise added to the data. Furthermore, the reconstructions will remain essentially the same even with much higher amounts of noise in the data. This is not a surprise since the evanescent modes are typically sensitive with noise but the sampling method only uses propagating modes. The great robustness against noise in the data was also seen in the orthogonality sampling methods studied in [12, 19, 26].

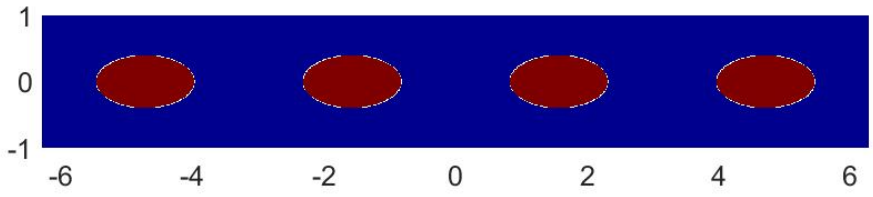

(a) True geometry in $(-2\pi, 2\pi)$.

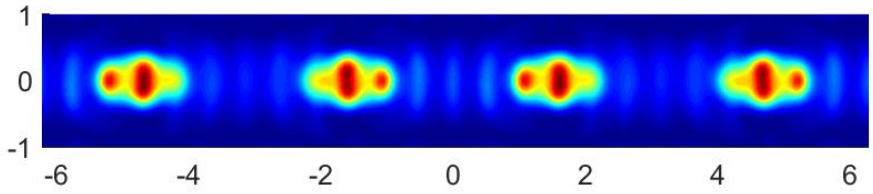

(b) Reconstruction with 32 incident sources.

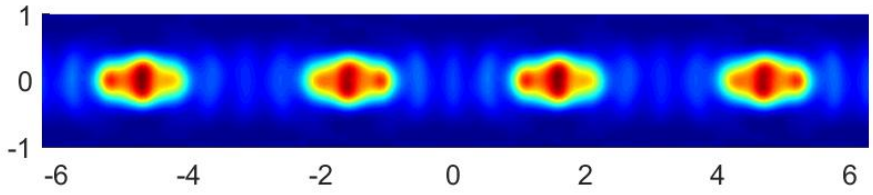

(c) Reconstruction with 64 incident sources.

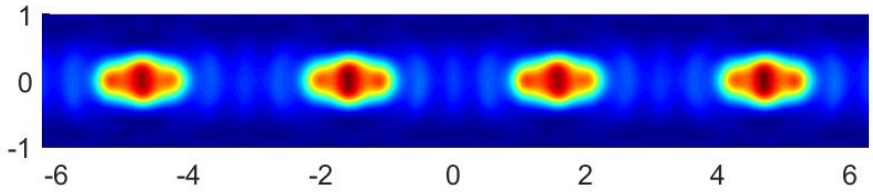

(d) Reconstruction with 128 incident sources.

Figure 4: Reconstruction with different numbers of incident sources.

4.4 Reconstruction with higher wave numbers (Figure 6)

Besides the reconstruction result for $k = 2\pi$ we test in this section the performance of the method for reconstructing extended scatterers with higher wave numbers ($k = 3\pi$, 5π, 6π). Here the parameters are chosen as $\alpha = 0$, exponent $p = 4$, 128 incident sources are used to generate the scattering data, and 20% noise added to the data. We can see from Figure 6 that the resolution of reconstructions improve as the wave number increases from 2π to 3π, which is reasonable. However, the reconstruction results are not better for $k = 5\pi$ and $k = 6\pi$. It is also known that as the wave number increases, the nonlinearity and ill-posedness of the inverse problem become more difficult to deal with. We can clearly notice some effects of

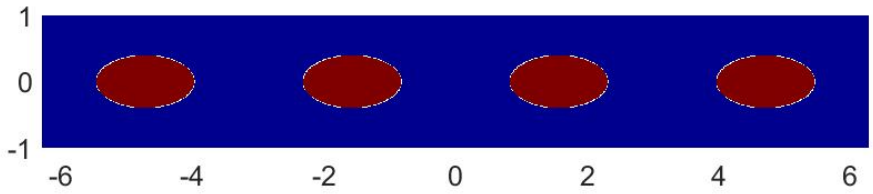

(a) True geometry in $(-2\pi, 2\pi)$.

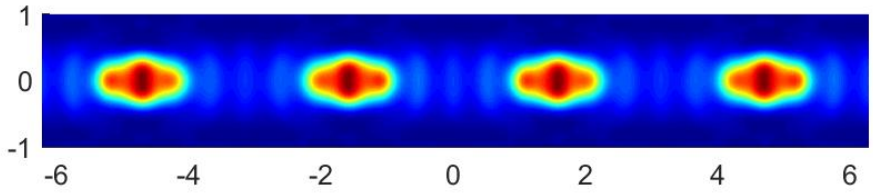

(b) Reconstruction with 10% noise.

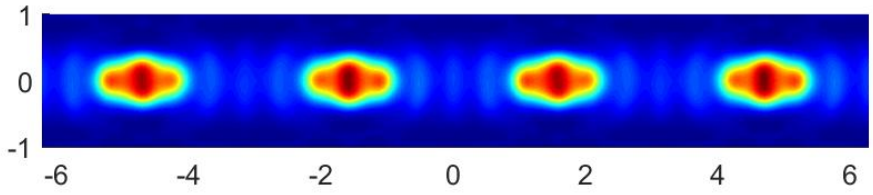

(c) Reconstruction with 20% noise.

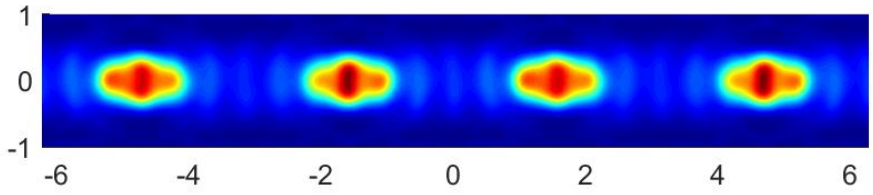

(d) Reconstruction with 40% noise.

Figure 5: Reconstruction with different levels of noise in the data.

large wave numbers in the reconstruction results for $k = 5\pi$ and $k = 6\pi$.

4.5 Reconstruction with different values of α and p (Figures 7–8)

In this section we test the performance of the method for different values of the parameters α and p. The other parameters are chosen as $k = 2\pi$, 128 incident sources are used to generate the scattering data, and 20% noise added to the data. From Figures 7–8, we can see that the sampling method works well for different values of α. Although the reconstructions look reasonable for exponents $p = 2$ and $p = 3$, the exponent $p = 4$ seems to be an ideal exponent

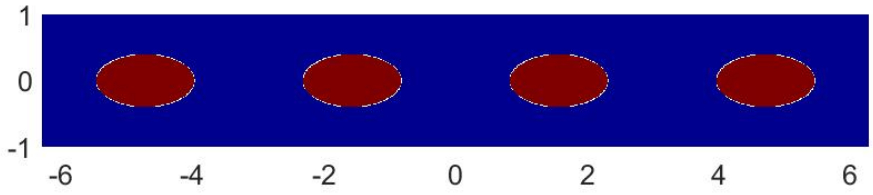

(a) True geometry in $(-2\pi, 2\pi)$.

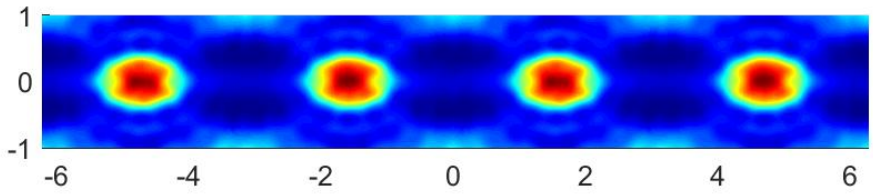

(b) Reconstruction with wave number $k = 3\pi$.

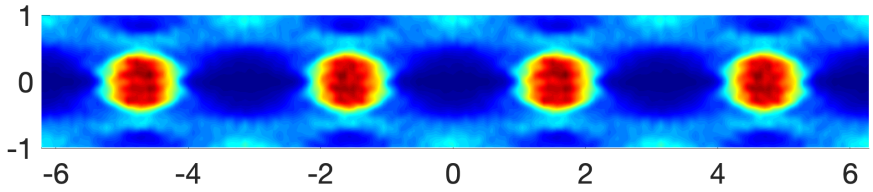

(c) Reconstruction with wave number $k = 5\pi$.

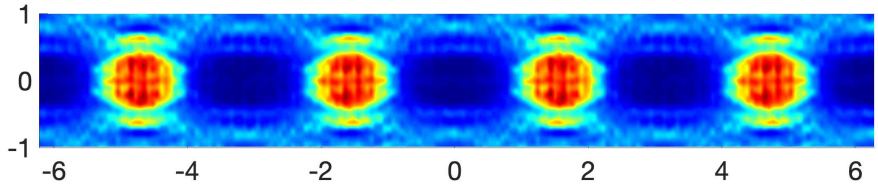

(d) Reconstruction with wave number $k = 6\pi$.

Figure 6: Reconstruction with higher wave numbers.

for the indicator function. With larger p the reconstructions will have cleaner background but lose some small details of the scatterers.

4.6 Reconstruction of different shapes and comparison with the factorization method and the orthogonality sampling method (Figures 9–12)

In this section we test the performance of the proposed sampling method for different shapes of periodic scatterers and compare its performance with those of the factorization method and the orthogonality sampling method. The parameters are chosen as $\alpha = 0$, wave number $k = 2\pi$, exponent $p = 4$, 128 incident sources are used to generate the scattering data, and 20% noise added to the data. It is obvious from all reconstructions in Figures 9–12 that the factorization method suffers severely from the 20% amount of noise added to the scattering data. Actually, the reconstructions of the factorization method can be greatly affected even with smaller amounts of noises (e.g. 5% or 7%). This unstable behavior of the factorization method in reconstructing periodic media was also reported in [1, 23]. The reconstructions of the orthogonality sampling method are as stable as those of the proposed sampling method but it is also clear from the pictures that the accuracy in the reconstructions of the orthogonality sampling method is much worse than that of the proposed sampling method. The proposed sampling method may provide reasonable reconstructions for different shapes considered in the test. This indicates a high efficiency of this sampling method.

Acknowledgement. This work was partially supported by NSF grants DMS-1812693 and DMS-2208293.

References

[1] T. Arens and N.I. Grinberg. A complete factorization method for scattering by periodic structures. *Computing*, 75:111–132, 2005.

[2] T. Arens and A. Kirsch. The factorization method in inverse scattering from periodic structures. *Inverse Problems*, 19:1195–1211, 2003.

[3] Tilo Arens. Scattering by biperiodic layered media: The integral equation approach. Habilitation Thesis, Universität Karlsruhe, 2010.

[4] G. Bao, T. Cui, and P. Li. Inverse diffraction grating of Maxwell's equations in biperiodic structures. *Optics Express*, 22:4799–4816, 2014.

[5] A.-S. Bonnet-Bendhia and F. Starling. Guided waves by electromagnetic gratings and non-uniqueness examples for the diffraction problem. *Math. Meth. Appl. Sci.*, 17:305–338, 1994.

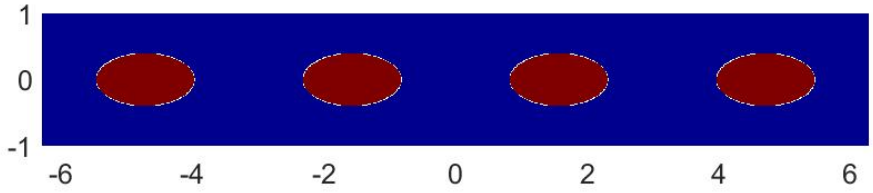

(a) True geometry in $(-2\pi, 2\pi)$.

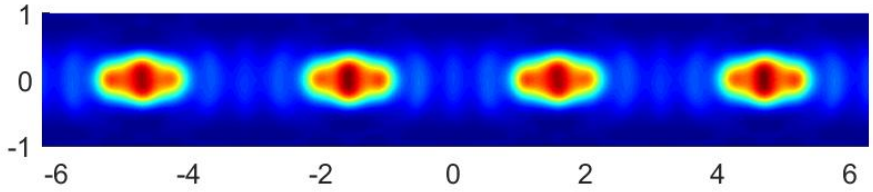

(b) Reconstruction with parameter $\alpha = 0$.

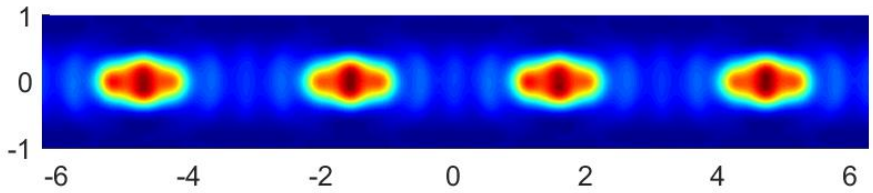

(c) Reconstruction with parameter $\alpha = \pi/3$.

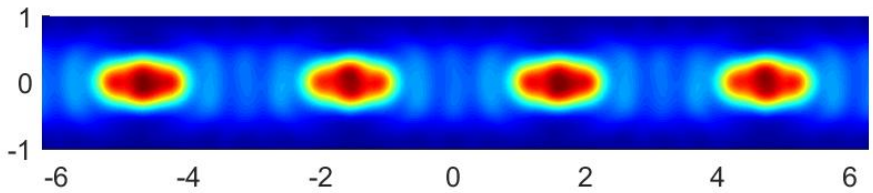

(d) Reconstruction with parameter $\alpha = \pi$.

Figure 7: Reconstruction with different values of parameter α.

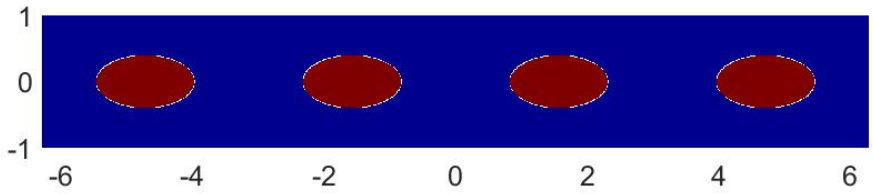

(a) True geometry in $(-2\pi, 2\pi)$.

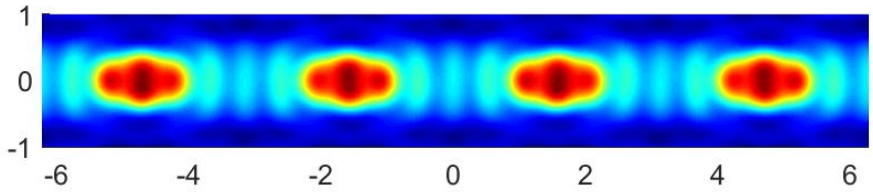

(b) Reconstruction with exponent $p = 2$.

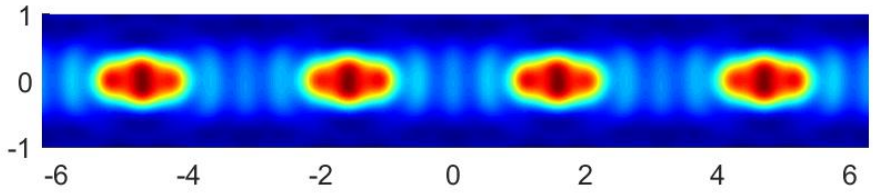

(c) Reconstruction with exponent $p = 3$.

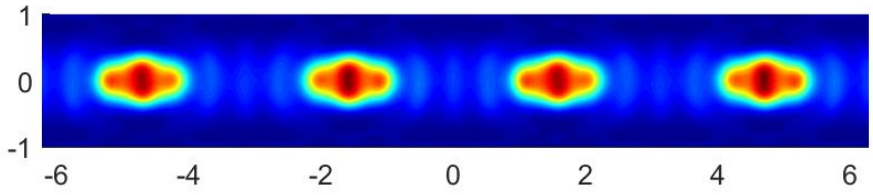

(d) Reconstruction with exponent $p = 4$.

Figure 8: Reconstruction with different exponents p in the indicator function.

[6] F. Cakoni, H. Haddar, and T.-P. Nguyen. New interior transmission problem applied to a single Floquet–Bloch mode imaging of local perturbations in periodic media. *Inverse Problems*, 35:015009, 2019.

[7] D. Colton and A. Kirsch. A simple method for solving inverse scattering problems in the resonance region. *Inverse Problems*, 12:383–393, 1996.

[8] W. Dorfler, A. Lechleiter, M. Plum, G. Schneider, and C. Wieners. *Photonic Crystals: Mathematical Analysis and Numerical Approximation*. Springer, Basel., 2012.

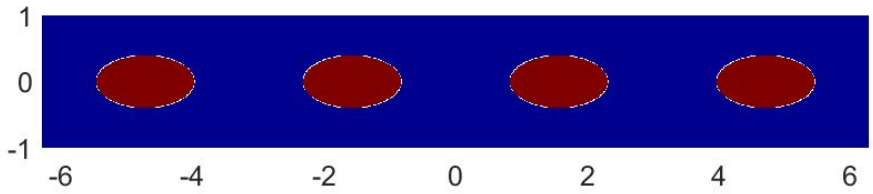

(a) True geometry in $(-2\pi, 2\pi)$.

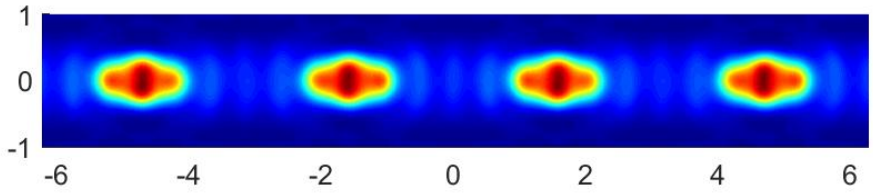

(b) Reconstruction by the proposed sampling method.

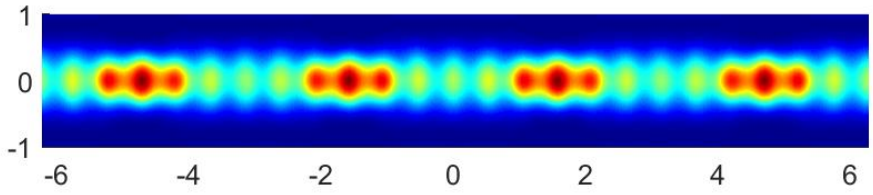

(c) Reconstruction by the orthogonality sampling method.

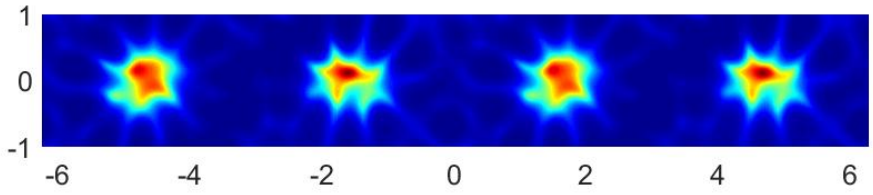

(d) Reconstruction by the factorization method.

Figure 9: Reconstruction of elliptical scatterers using different sampling methods.

[9] J. Elschner and G. Hu. An optimization method in inverse elastic scattering for one-dimensional grating profiles. *Commun. Comput. Phys.*, 12:1434–1460, 2012.

[10] R. Griesmaier. Multi-frequency orthogonality sampling for inverse obstacle scattering problems. *Inverse Problems*, 27:085005, 2011.

[11] H. Haddar and T.-P. Nguyen. Sampling methods for reconstructing the geometry of a local perturbation in unknown periodic layers. *Comput. Math. Appl.*, 74:2831–2855, 2017.

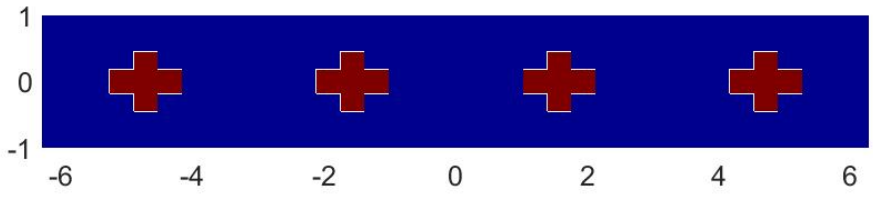

(a) True geometry in $(-2\pi, 2\pi)$.

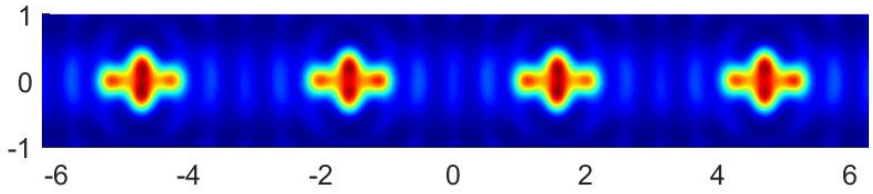

(b) Reconstruction by the proposed sampling method.

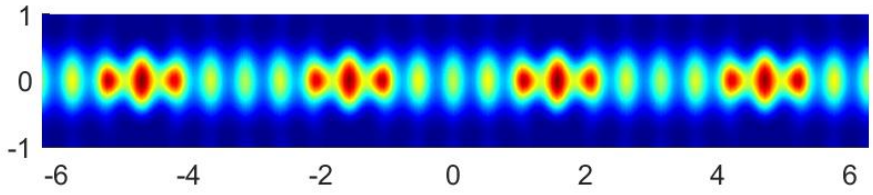

(c) Reconstruction by the orthogonality sampling method.

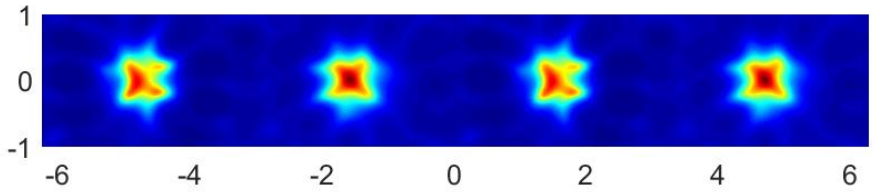

(d) Reconstruction by the factorization method.

Figure 10: Reconstruction of cross-shaped scatterers using different sampling methods.

[12] I. Harris and D.-L. Nguyen. Orthogonality sampling method for the electromagnetic inverse scattering problem. *SIAM J. Sci. Comput.*, 42:B72–B737, 2020.

[13] K. Ito, B. Jin, and J. Zou. A direct sampling method to an inverse medium scattering problem. *Inverse Problems*, 28:025003, 2012.

[14] K. Ito, B. Jin, and J. Zou. A direct sampling method for inverse electromagnetic medium scattering. *Inverse Problems*, 29:095018, 2013.

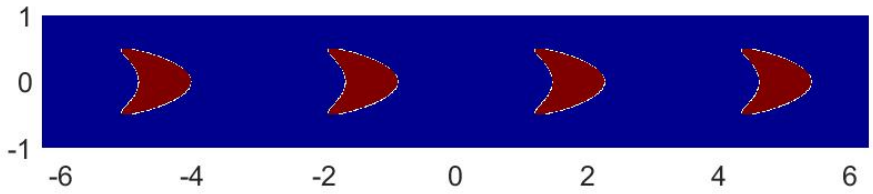

(a) True geometry in $(-2\pi, 2\pi)$.

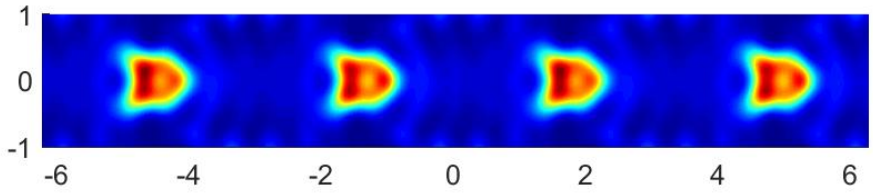

(b) Reconstruction by the proposed sampling method.

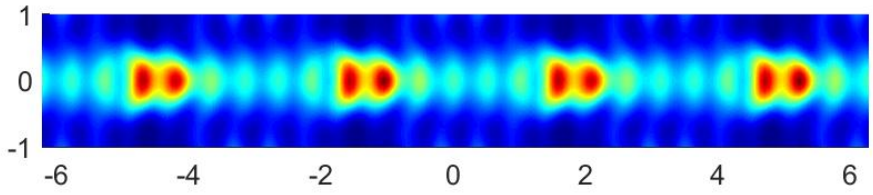

(c) Reconstruction by the orthogonality sampling method.

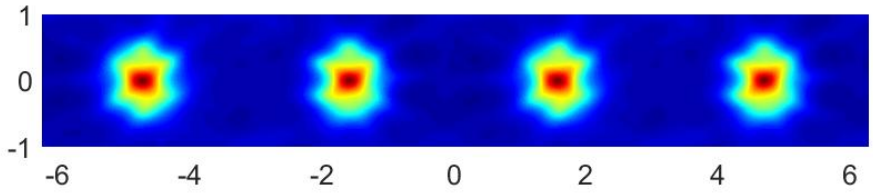

(d) Reconstruction by the factorization method.

Figure 11: Reconstruction of kite-shaped scatterers using different sampling methods.

[15] X. Jiang and P. Li. Inverse electromagnetic diffraction by biperiodic dielectric gratings. *Inverse Problems*, 33:085004, 2017.

[16] S. Kang, M. Lambert, and W.-K. Park. Direct sampling method for imaging small dielectric inhomogeneities: analysis and improvement. *Inverse Problems*, 34:095005, 2018.

[17] A. Kirsch. Characterization of the shape of a scattering obstacle using the spectral data of the far field operator. *Inverse Problems*, 14:1489–1512, 1998.

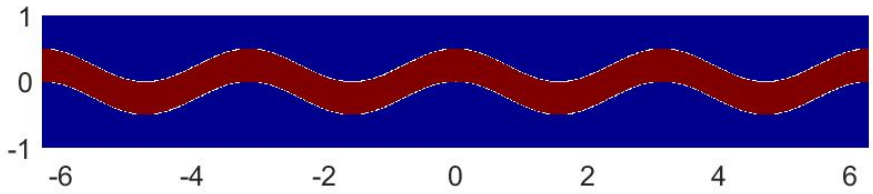

(a) True geometry in $(-2\pi, 2\pi)$.

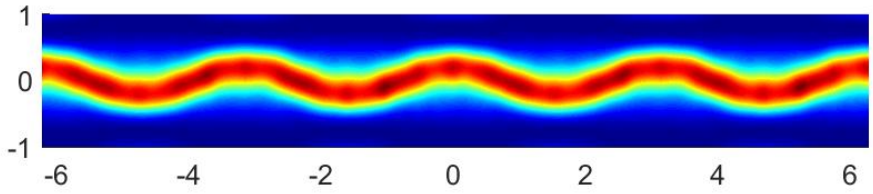

(b) Reconstruction by the proposed sampling method.

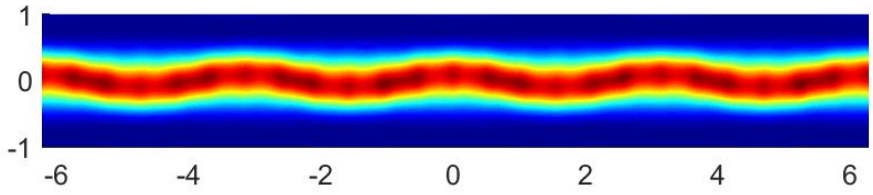

(c) Reconstruction by the orthogonality sampling method.

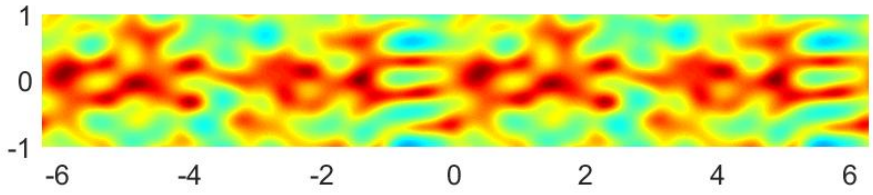

(d) Reconstruction by the factorization method.

Figure 12: Reconstruction of a sinusoidal scatterer using different sampling methods.

[18] A. Kirsch and N.I. Grinberg. *The Factorization Method for Inverse Problems*. Oxford Lecture Series in Mathematics and its Applications 36. Oxford University Press, 2008.

[19] T. Le, D.-L. Nguyen, H. Schmidt, and T. Truong. Imaging of 3D objects with experimental data using orthogonality sampling methods. *Inverse Problems*, 38:025007, 2022.

[20] A. Lechleiter and D.-L. Nguyen. Factorization method for electromagnetic inverse scattering from biperiodic structures. *SIAM J. Imaging Sci.*, 6:1111–1139, 2013.

[21] A. Lechleiter and D.-L. Nguyen. A trigonometric Galerkin method for volume integral equations arising in TM grating scattering. *Adv. Comput. Math.*, 40:1–25, 2014.

[22] D.-L. Nguyen. Shape identification of anisotropic diffraction gratings for TM-polarized electromagnetic waves. *Appl. Anal.*, 93:1458–1476, 2014.

[23] D.-L. Nguyen. The Factorization method for the Drude-Born-Fedorov model for periodic chiral structures. *Inverse Probl. Imaging*, 10:519–547, 2016.

[24] D.-L. Nguyen and T. Truong. Imaging of bi-anisotropic periodic structures from electromagnetic near field data. *J. Inverse Ill-Posed Probl.*, 30:205–219, 2022.

[25] T.-P. Nguyen. Differential imaging of local perturbations in anisotropic periodic media. *Inverse Problems*, 36:034004, 2020.

[26] R. Potthast. A study on orthogonality sampling. *Inverse Problems*, 26:074015, 2010.

[27] K. Sandfort. *The factorization method for inverse scattering from periodic inhomogeneous media*. PhD thesis, Karlsruher Institut für Technologie, 2010.

[28] J. Yang, B. Zhang, and R. Zhang. A sampling method for the inverse transmission problem for periodic media. *Inverse Problems*, 28:035004, 2012.